Molecular Crystals and Liquid Crystals

ISSN: (Print) (Online) Journal homepage: www.tandfonline.com/journals/gmcl20

Synthesis, crystal structure, Hirshfeld surface analysis, energy frameworks, and DFT calculations of (2*e*)-3-(dimethylamino)-1-[5-methyl-1-(4-nitrophenyl)-1*h*-1,2,3-triazol-4-yl]prop-2-en-1-one

M. K. Usha, T. N. Lohith, M. Manjula, Shobhitha Shetty, Balakrishna Kalluraya, D. Revannasiddaiah & M. A. Sridhar

To cite this article: M. K. Usha, T. N. Lohith, M. Manjula, Shobhitha Shetty, Balakrishna Kalluraya, D. Revannasiddaiah & M. A. Sridhar (10 Mar 2024): Synthesis, crystal structure, Hirshfeld surface analysis, energy frameworks, and DFT calculations of (2*e*)-3-(dimethylamino)-1-[5-methyl-1-(4-nitrophenyl)-1*h*-1,2,3-triazol-4-yl]prop-2-en-1-one, Molecular Crystals and Liquid Crystals, DOI: 10.1080/15421406.2024.2326337

To link to this article: https://doi.org/10.1080/15421406.2024.2326337

Taylor & Francis
Taylor & Francis Group

MOLECULAR CRYSTALS AND LIQUID CRYSTALS
https://doi.org/10.1080/15421406.2024.2326337

Synthesis, crystal structure, Hirshfeld surface analysis, energy frameworks, and DFT calculations of (2*e*)-3-(dimethylamino)-1-[5-methyl-1-(4-nitrophenyl)-1*h*-1,2,3-triazol-4-yl]prop-2-en-1-one

M. K. Usha[a,b], T. N. Lohith[c,d], M. Manjula[e], Shobhitha Shetty[f], Balakrishna Kalluraya[g], D. Revannasiddaiah[b], and M. A. Sridhar[d]

[a]Editorial Support Division, Molecular Connections Pvt. Ltd, Bengaluru, India; [b]P.G. Department of Physics, St. Philomena's College (Autonomous), Mysuru, India; [c]Department of Physics, The National Institute of Engineering, Mysuru, India; [d]Department of Studies in Physics, University of Mysore, Mysuru, India; [e]Department of Physics, Jain University School of Sciences, Bengaluru, India; [f]Department of Studies in Chemistry, A. J. Institute of engineering and technology, Mangaluru, India; [g]Department of Studies in Chemistry, Mangalore University, Mangaluru, India

ABSTRACT

A novel triazole derivative was synthesized and characterized by various spectroscopic techniques such as FTIR, NMR and single crystal X-ray diffraction study. The title compound crystallizes in the triclinic space group $P\bar{1}$ and exhibits inter-molecular hydrogen bonds of the type C–H … O and C–H … N. Hirshfeld surface analysis shows that the major intermolecular interaction is mainly due to H … H contacts. DFT calculations were performed to study their electronic properties. QTAIM and NCI studies were used to investigate the weak interactions in five triazole derivatives including the title compound.

KEYWORDS

Crystal structure; DFT; Hirshfeld surface analysis; NCI; QTAIM; Triazoles

1. Introduction

The heterocyclic compounds containing triazole moieties have shown significant activity as drugs in treating various diseases. According to the position of nitrogen atoms triazole exists in two isomeric forms, namely 1,2,3-triazole and 1,2,4-triazole. These are essential aromatic heterocyclic chemical compounds with molecular formula $C_2H_3N_3$, which have a five-membered ring of two carbon atoms and three nitrogen atoms [1]. The triazole compounds and their fused heterocyclic derivatives are interesting in synthetic and biological fields [2]. These compounds are found to possess antifungal [3], antibacterial [4], cytotoxicity [5], anti-mycobacterial [6], antiviral, anticancer, and anti-inflammatory activities. 1,2,3-triazole and its derivatives are well known due to their chemo-therapeutical value. They are used as DNA cleaving agents and potassium channel activators [7]. They are also used as analytical reagents, photographic chemicals, polymer synthesis and light emitting diodes (electroluminescent devices).

CONTACT M. K. Usha usha.mk@gmail.com Editorial Support Division, Molecular Connections Pvt. Ltd., Bengaluru, India

Supplemental data for this article can be accessed online at https://doi.org/10.1080/15421406.2024.2326337.

Enaminones are compounds that contain an amino group linked through a C = C to a carbonyl group and can be easily synthesized in laboratories. Their major use is as reagents and synthetic intermediates. The synthesis procedure described here is as per our previous research on synthesis of various bio-active triazole derivatives [8]. Literature survey thus reveals that a compound that belongs to the class of enaminones and 1,2,3-triazole can have significant pharmaceutical value. In view of the above discussion, one triazole derivative was synthesized, crystallized, and structure was elucidated using single crystal X-ray diffraction. The non-covalent interactions were investigated and compared with four other 1,2,3-triazole derivatives whose synthesis has been reported in our previous work [8].

2. Materials and methods

2.1. Synthesis

Chemicals required for synthesis of the title compound were purchased from Sigma Aldrich Chemical Corporation. Melting point was determined in open capillary tube and is uncorrected. The title compound (C1) was prepared by refluxing a mixture of 1-[5-methyl-1-(4-nitrophenyl)-1*H*-1,2,3-triazol-4-yl]ethanone (2.46 g, 1.00×10^{-2} mol) and dimethyl formamide dimethyl acetal (2.38 g, 2.00×10^{-2} mol). The reaction mixture was refluxed for 4 h and then it was cooled to room temperature. The final product separated was filtered and dried. It was then recrystallized using ethanol as a solvent. Suitable crystals for X-ray analysis were obtained from slow evaporation method using ethanol as a solvent. The scheme of synthesis is shown in Figure 1.

Along with the title compound (**C1**), the following four triazole derivatives were used in the present work for comparative studies: **C2**: (2*E*)-3-(dimethylamino)-1-[5-methyl-1-(4-bromophenyl)-1*H*-1,2,3-triazol-4-yl]prop-2-en-1-one; **C3**: (2*E*)-3-(dimethylamino)-1-[5-methyl-1-(4-chlorophenyl)-1*H*-1,2,3-triazol-4-yl]prop-2-en-1-one; **C4**: (2*E*)-3-(dimethylamino)-1-[5-methyl-1-(4-methoxyphenyl)-1*H*-1,2,3-triazol-4-yl]prop-2-en-1-one and **C5**: 4-{4-[(2*E*)-3-(dimethylamino)-prop-2-enoyl]-5-methyl-2*H*-1,2,3-triazol-2-yl]

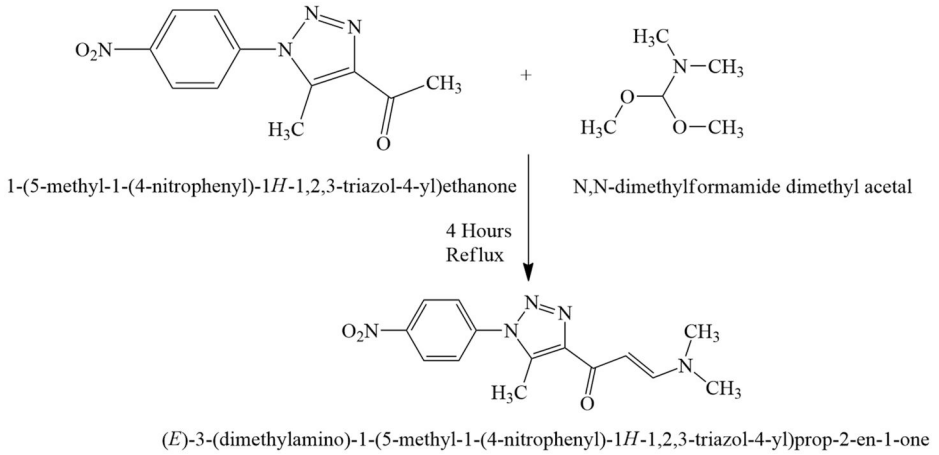

Figure 1. Synthesis pathway of the title compound.

benzene-1-sulfonamide. They contain bromophenyl (C2), chrolophenyl (C3), methoxyphenyl (C4), and sulfanamide (C5) groups respectively in place of nitrophenyl in the title compound. Chemical synthesis of these four compounds (C2 to C5) are reported in our previous work [8].

2.2. Spectroscopy

^{1}HNMR spectra was recorded on a Bruker AMX-300/AMX-400 (300/400 MHz) spectrometer using DMSO-d6 as solvent and TMS as an internal standard. All chemical shifts values are reported in *d*-scale downfield from TMS. The infrared spectrum of the synthesized compound was recorded in the region 4000–400 cm^{-1} using a KBr pellet on a MATSON-1000 model FT-IR spectrometer. Mass spectra of the compound was recorded in Agilent mass spectrometer operating at 20 eV and C, H, N analysis was carried out on a Schimadzu Elementar Vario-EL (Elementar-III) model. Homogeneity of the compound was checked by TLC on silica gel plates.

2.3 X-ray diffraction

The crystals of the title compound were pale yellow in color. A crystal of size 0.30 mm × 0.20 mm × 0.20 mm was carefully chosen for X-ray diffraction study after checking it for visible defects using a microscope. Crystallographic data were collected using a Bruker Xcalibur diffractometer having Sapphire three CCD plate operating with Cu$K\alpha$ radiation of wavelength 1.5417 Å. Data reduction and absorption correction were carried out using the APEX 2 package [9]. *SHELXS* was used to solve the crystal structure using intrinsic phasing and refinement was carried out using *SHELXL* [10] on the basis of least square refinement. All the non-hydrogen atoms were refined anisotropically and the hydrogen atoms were placed at chemically acceptable positions. The geometrical calculations were carried out using the program *PLATON* [11]. The molecular and packing diagrams were generated using the software *MERCURY* [12].

2.4. Computational details

CrystalExplorer 17.5 [13] was used to create the molecular Hirshfeld surfaces and associated two-dimensional fingerprint plots for all the molecules. The intermolecular interactions that cause molecular packing in the crystal can be seen and studied using graphical displays of the molecular Hirshfeld surface. The ratio of the electron distribution of a sum of spherical atoms for the molecule to the comparable sum over the crystal is known as the Hirshfeld surface [14]. The Hirshfeld surface projected over dnorm is highlighted in Figure 2. The normalized contact distance d_{norm} is

$$d_{norm} = \frac{d_i - r_i^{vdW}}{r_i^{vdW}} + \frac{d_e - r_e^{vdW}}{r_e^{vdW}} \tag{1}$$

where d_i and d_e are the distances from the surface to the nearest nuclei internal and external to the surface respectively; r_i^{vdW} and r_e^{vdW} are the van der Waal's radii of the atoms internal and external to the surface respectively [15].

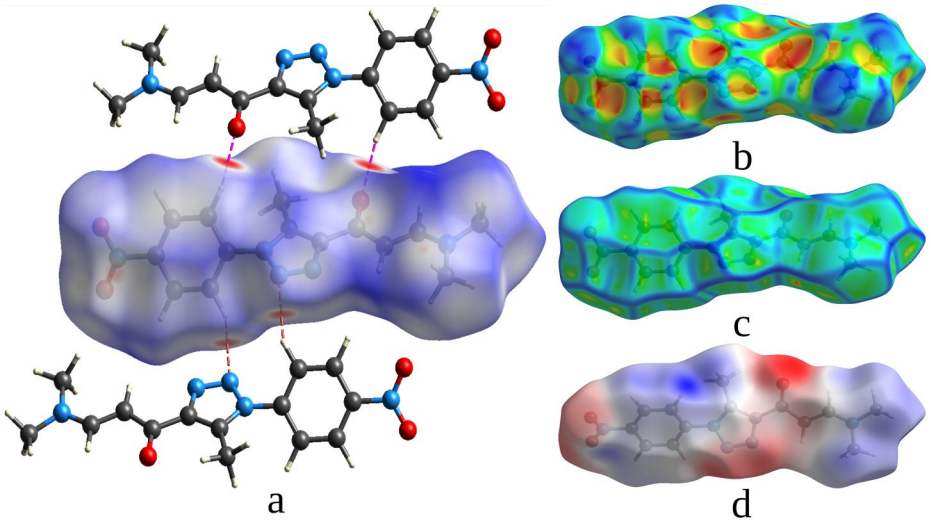

Figure 2. (a) d_{norm} surface (b) shape index (c) curvedness, and (d) electrostatic potential surface of the triazole derivative.

Also, the intermolecular interaction energies and the total interaction energy between the molecules were calculated using the method B3LYP/6-31G(d,p) energy model. The total interaction energy is calculated using the equations,

$$E_{tot} = E_{ele} + E_{pol} + E_{dis} + E_{rep} \tag{2}$$

$$E_{tot} = k_{ele}E'_{ele} + k_{pol}E'_{pol} + k_{dis}E'_{dis} + k_{rep}E'_{rep} \tag{3}$$

where E'_{ele} represents the electrostatic energy of interaction, E'_{pol} is the polarization energy, E'_{dis} represents the dispersion energy, E'_{rep} repulsion energy. K is the scale factor determined by the calibration against quantum mechanical results. These interaction energy values were employed to construct the three-dimensional energy frameworks which visualize the packing of the molecules in the crystal structure [16, 17].

The structure of the studied molecule was optimized in the gas phase using ωB97X exchange–correlation functional with Grimme D3 dispersion corrections as well as a Becke–Johnson damping function (D3-BJ) method at the 6-311 + G(d,p) [18] for all atoms with the help of the Gaussian 09 [19] software. Frequency analysis was used to check geometry optimizations to make sure they were at the potential energy surface's minimum (PES). The findings demonstrated that there were no imaginary frequencies. The Koopman's approximation was used to determine the energy gap between the highest occupied and lowest unoccupied molecular orbitals (HOMO–LUMO), as well as the global reactive parameters. In Gaussview 06 [20], 3D molecular orbitals were viewed. To ascertain the possible reactive sites and charge distribution of the molecules, the molecular electrostatic potential (MEP) analysis was performed. In order to understand the electron density values, the bond critical points (BCPs), and the weak interactions present in the molecules, the quantum theory of atoms in molecules (QTAIM) and reduced density gradient (RDG) investigations were conducted [21]. The Multiwfn 3.7 [22] package was used to do the appropriate calculations for MEP, QTAIM, and RDG, and the Visual Molecular Dynamics [23] software was used to show the results.

3. Results and discussion

3.1. Spectral analysis

Infrared (IR) and hydrogen NMR (^{1}HNMR) spectroscopy were used to check the functional groups present in the compound. The chemical composition was checked using elemental analysis. The results obtained from these techniques are given below. Spectroscopic characterization of C2, C3, C4 and C5 are reported in our previous work [8] and are not repeated here.

3.1.1. IR

The following IR absorption peaks were observed in the IR spectrum. The carbonyl absorption band was seen at 1645 cm^{-1} while the C–H stretching was observed at 2980 cm^{-1}. The intense absorption peak appears at 1550–1470 cm^{-1} indicates the presence of $–NO_2$ group in the molecule. Further, appearance of vibrational peaks at 1220, 1340, 1650, 1735, and 2140 cm^{-1} indicates the presence of tertiary amine (–N=), $N–CH_3$, alkene (C=C), carbonyl (C=O), and N–N=N groups respectively.

3.1.2. ^{1}H NMR

In the ^{1}H-NMR spectrum of this compound, the two N-methyl groups appeared as two singlets each integrating for three protons at δ 2.96 and 3.18 thereby indicating the non-equivalency of these two methyl group. The olefinic CH protons come into resonance as doublets with coupling constant $J = 12.4$ Hz each integrating for one proton at δ, 5.89 and 7.82 respectively. The methyl group attached to the triazole ring appeared as a singlet at δ, 2.71 integrating for three protons. The meta and ortho protons of p-nitrophenyl group appeared as two doublets with $J = 8.8$ Hz each integrating for two protons at δ, 8.12 and 8.27, respectively.

Yield: 71%. M.P. 148-149^{0}C. (Molecular Formula - $C_{14}H_{15}N_5O_3$.)

3.1.3. Elemental analysis

CHN elemental analysis was carried out in order to confirm the chemical composition of the synthesized compound. The obtained results are: C-55.83(55.81), H-5.00(5.02), N-23.22(23.24), where the calculated percentages of elements are given in brackets. The differences between experimental and calculated percentages of Carbon (C), Hydrogen (H) and Nitrogen (N) are very small and within the experimental errors. This confirms that the product formation is in stoichiometric proportion.

3.2. Single crystal X-ray diffraction

From X-ray diffraction study, the title compound (**C1**) is found to crystallized in the triclinic crystal system in space group $P\bar{1}$. with cell parameters $a = 7.8179(14)$ Å, $b = 10.1899(17)$ Å, $c = 10.3734(17)$ Å, $\alpha = 109.603(7)^\circ$, $\beta = 90.114(7)^\circ$, $\gamma = 108.043(8)^\circ$, $Z = 2$ and $V = 735.0(2)$ Å^3. A total of 203 parameters were refined with 2340 unique reflections which converged the residual to $R = 0.0399$. The details of crystal data and structure refinement are given in Table 1. Figure 3 shows the *ORTEP* diagram of the

Table 1. Crystal data and structure refinement details of the title compound.

Parameters	Values
CCDC	2040631
Empirical formula	$C_{14}H_{15}N_5O_3$
Formula weight	301.31
Temperature	293
Wavelength	1.54178 Å
Reflections for cell determination	2340
θ range for above	4.56°–64.55°
Crystal system	triclinic
Space group	$P\bar{1}$
Cell dimensions	$a = 7.8179(14)$ Å
	$b = 10.1899(17)$ Å
	$c = 10.3734(17)$ Å
	$\alpha = 109.603(7)°$
	$\beta = 90.114(7)°$
	$\gamma = 108.043(8)°$
Volume	735.0(2) Å^3
Z	2
Density(calculated)	1.352 Mg m^{-3}
Absorption coefficient	0.806 mm^{-1}
F_{000}	316
Crystal size	0.30 × 0.20 × 0.20 mm
θ range for data collection	4.56°–64.55°
Index ranges	$-9 \leq h \leq 9$
	$-11 \leq k \leq 9$
	$-12 \leq l \leq 11$
Reflections collected	5309
Independent reflections	2340 [$R_{int} = 0.019$]
Absorption correction	Multi-scan
Refinement method	full matrix least-squares on F^2
Data / restraints / parameters	2340/0/203
Goodness-of-fit on F^2	1.039
Final R indices [$I > 2\ \sigma(I)$]	$R1 = 0.0399$, $wR2 = 0.1048$
R indices (all data)	$R1 = 0.0423$, $wR2 = 0.1071$
Extinction coefficient	0.015(4)
Largest diff. peak and hole	0.160; −0.179 e Å^{-3}

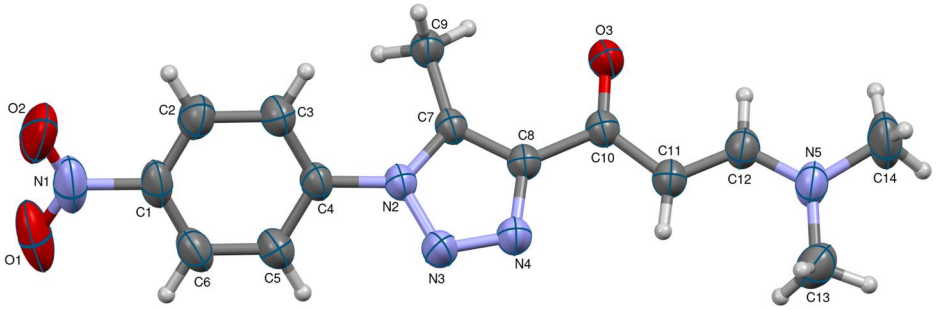

Figure 3. *ORTEP* diagram of the title compound with 50% probability ellipsoids.

molecule with thermal ellipsoids drawn at 50% probability. Selected bond lengths and bond angles, and torsion angles are listed in the Tables 2 and 3, respectively. All the bond lengths and bond angles are comparable with compounds having similar structure [5, 15, 16]. Hydrogen bond geometry details are provided in Table 4. The intermolecular hydrogen bond interactions of type C3–H3 … O3 and C5-H5 … N3 exhibited by the

Table 2. Selected bond lengths and bond angles.

Atoms	Bond length (Å)	Atoms	Bond angle (°)
O1–N1	1.216(2)	O1–N1–O2	123.9(2)
C1–C2	1.371(2)	O1–N1–C1	118.14(19)
N1–C1	1.470(3)	N3–N2–C4	118.38(12)
N2–N3	1.367(2)	N3–N2–C7	111.06(12)
N3–N4	1.2983(19)	C4–N2–C7	130.54(13)
N2–C7	1.3581(17)	N2–N3–N4	107.06(12)
C7–C8	1.384(2)	N1–C1–C2	118.83(18)
C11 –C12	1.355(2)	C2–C1–C6	122.31(17)
C7–C9	1.484(2)	O3–C10–C8	118.21(14)
C10–C11	1.432(2)	C12–N5–C14	121.09(17)
O3–C10	1.2394(18)	C10–C11–C12	119.05(14)
N5–C14	1.451(2)	C13–N5–C14	117.57(17)

Table 3. Selected Torsion angles.

Atoms	Angle (°)	Atoms	Angle (°)
O1–N1–C1–C2	165.1(2)	C6–C1–C2–C3	0.4(3)
O1–N1–C1–C6	−15.3(2)	N1–C1–C6–C5	179.3(2)
O2–N1–C1–C2	−15.1(3)	C2–C1–C6–C5	−1.1(3)
O2–N1–C1–C6	164.6(2)	C1–C2–C3–C4	0.9(2)
C4–N2–N3–N4	178.8(1)	C2–C3–C4–N2	179.9(2)
C7–N2–N3–N4	0.3(2)	C2–C3–C4–C5	−1.6(2)
N3–N2–C4–C3	138.0(2)	N2–C4–C5–C6	179.5(1)
N3–N2–C4–C5	−40.6(2)	C3–C4–C5–C6	1.0(2)

Table 4. Hydrogen-bond geometry.

D–H … .A	D - H	H … A	D … A	D … A	Symmetry
C3–H3 … O(3)	0.93	2.35	3.249(2)	163	−x,1 − y,1 − z
C5–H5 … N(3)	0.93	2.49	3.349(2)	153	−x,−y,−z
C9–H9A … O(1)	0.96	2.50	3.450(2)	169	1 − x,1 − y,−z

adjacent molecules construct R_2^2 (16) and R_2^2 (10) supramolecular synthon respectively, leading to 1D molecular chains (Figure 4).

The phenyl ring C1–C6 and triazole ring N2–N3–N4–C8–C7 are highly planar and *sp2* hybridized. The maximum deviation from the mean plane in these rings are for atoms C3(0.0079(18) Å) and N4(−0.0018(15) Å) respectively. The angle between least square planes containing these rings is 41.9 Å and hence they are *syn-clinal*. Interactions between N–O–phenyl ring provides stability to the crystal structure.

The molecules are stacked in anti-parallel fashion forming interpenetrating layers as shown in Figure 5. The plane containing phenyl rings of two molecules belonging to alternate layers are parallel to each other and are stacked on top of one another. The plane containing triazole rings of molecules of adjacent layers are parallel to each other with the triazole rings oriented in anti-parallel fashion. The inter-planar distance between molecules is 3.596 Å which was measured with reference to the plane containing phenyl ring. The intermolecular distance between two neighboring molecules in each layer is 5.497 Å.

3.3. Hirshfeld surface analysis

The d_{norm} surface of the triazole molecule in the asymmetric unit of the crystal structure has been displayed in Figure 2a. The bright red spots emerged on d_{norm} surface

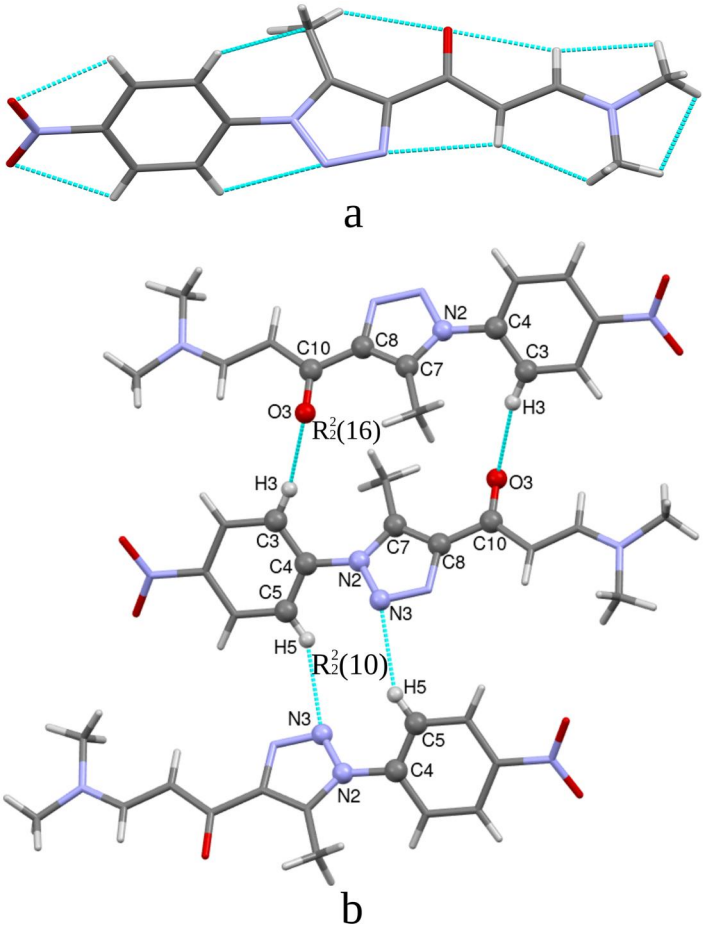

Figure 4. (a) Various intramolecular interactions present in the molecule (b) C–H … O and C–H … N intermolecular interactions between adjacent molecules.

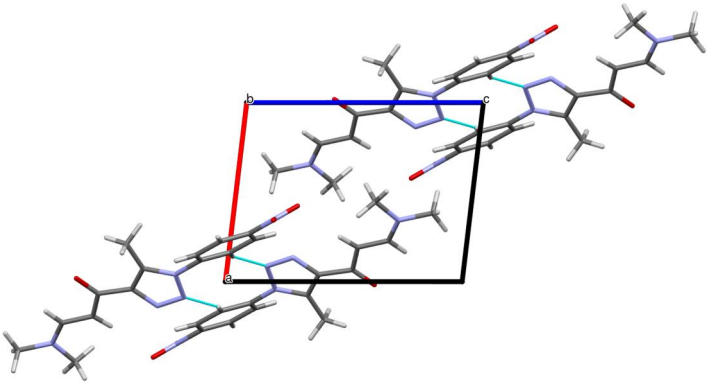

Figure 5. Packing diagram of the molecules showing anti-parallel arrangement of molecules in neighboring layers and intermolecular hydrogen bonds along crystallographic *b*-axis.

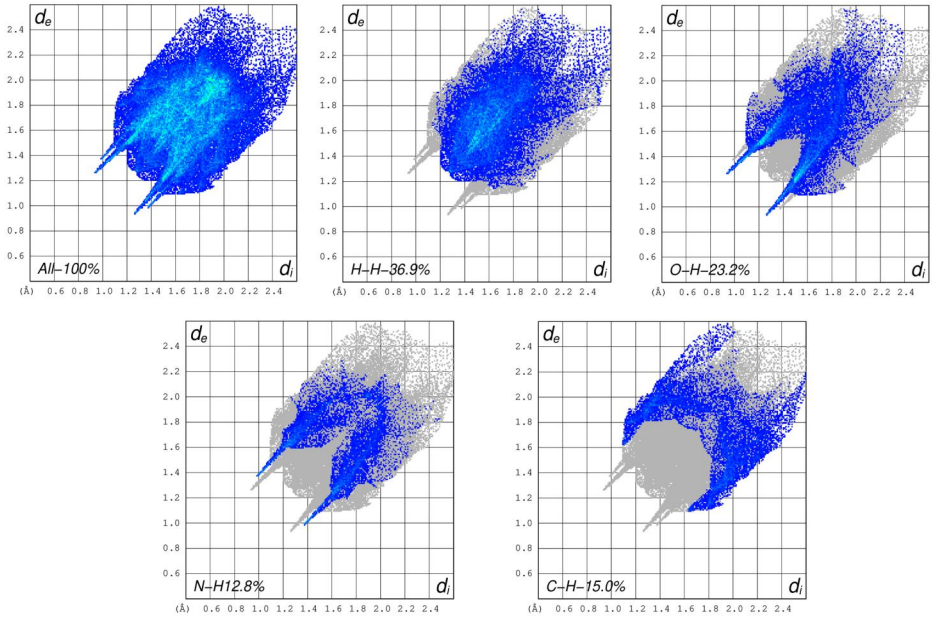

Figure 6. The relative major contributions of various intermolecular contacts to the Hirshfeld surface area of the title structure.

clearly indicates the existence of intermolecular hydrogen bond interactions, and have been shown in the supramolecular ring motifs present in the molecule. From Figure 2b, one can observe that the molecules are stacked by π -π interactions as adjacent red and blue patches appeared on the shape index surface. Also, N-O … π interactions are evident on the Hirshfeld surface as a large flat region across the molecule, which is clearly visible on the curvedness surface of the molecule (Figure 2c). Figure 2d highlights the electrostatic potential regions like electropositive (blue) and electronegative (red) regions on the surface. The appearance of red colored regions around the oxygen atoms of the nitro group, carbonyl group, and around the nitrogen atoms of the triazole ring indicate the electronegative spots, and the blue (hydrogen bond donors) colored regions near the dimethylamine and around hydrogen atoms present in the molecule indicate the electropositive spot.

The two-dimensional fingerprint plots are examined to obtain individual contribution of H … H (36.9%), O … H (23.2%), N … H (12.8%), and C … H (15.0%) intermolecular contacts to the total Hirshfeld surface as shown in Figure 6. The pair of large spikes in the O … H and short spikes in the N … H fingerprint plots corresponds to the O-H and N-H intermolecular contacts respectively, and revealed the occurrence of weak hydrogen bond interactions. The blue-green region on the fingerprint plot signifies the existence of π -π and N-O … π interactions in the title molecule.

3.4. Interaction energy and 3D energy frameworks

The software *CrystalExplorer 17.5* was employed to compute the interaction energy between molecules in the most effective way by creating a molecular cluster with a

radius of 3.8 around the chosen molecule, as shown in Figure 7 [24]. The B3LYP/6-31G(d,p) energy model was used for the energy framework calculations with the scale factors E_{tot}: k_{ele} = 1.057, k_{pol} = 0.740, k_{dis} = 0.871, and k_{rep} = 0.618. This method involved using symmetry operations to compute molecular wave functions and generate electron densities of the cluster of molecules present around the chosen molecule.

The crystallographic symmetry operations and the corresponding molecular interaction energies are summarized in Table 5. The light blue colored molecule with symmetry operation (*-x*, *-y*, *-z*) located at distance of 5.77 Å from the centroid of the

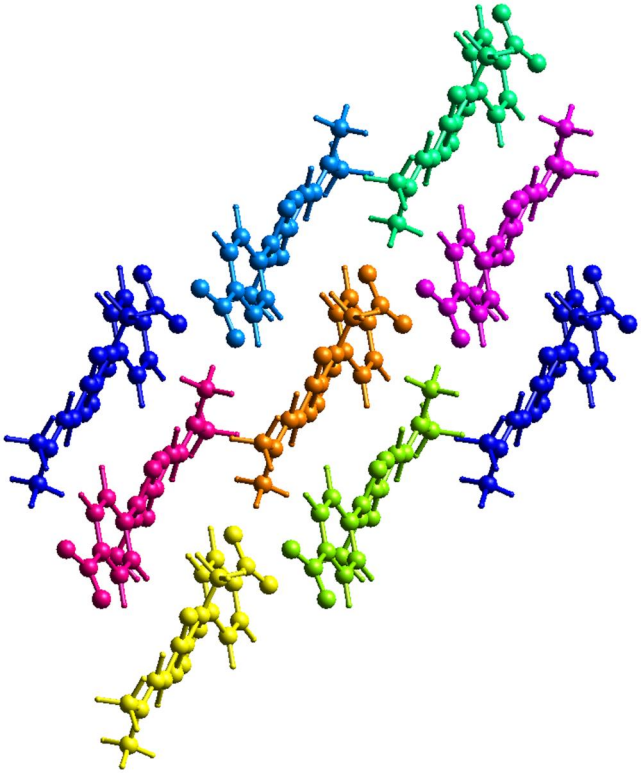

Figure 7. Molecular interactions between the selected molecule (at the center) and the molecules present in a cluster of radius 3.8 Å.

Table 5. Molecular interaction energies (kJ/mol) of the cluster of molecules.

	N	Symmetry operations	R in Å	E_ele	E_pol	E_dis	E_rep	E_tot
	1	−x, −y, −z	6.13	−40.3	−8.2	−31.1	34.7	−54.3
	1	x, y, z	10.37	−17.3	−5.3	−24.9	17.6	−33.0
	0	x, y, z	17.16	−8.1	−1.6	−5.7	5.2	−11.5
	1	−x, −y, −z	8.20	3.7	−3.6	−55.7	22.4	−33.5
	1	−x, −y, −z	10.53	−19.9	−4.6	−32.9	24.0	−38.1
	1	x, y, z	10.75	0.5	−0.8	−7.6	2.6	−5.0
	0	−x, −y, −z	8.63	3.2	−1.9	−28.1	12.7	−14.7
	0	−x, −y, −z	5.77	−40.8	−12.2	−45.5	49.7	−61.0
	1	x, y, z	13.00	3.0	−0.4	−3.3	0.1	0.1
	1	−x, −y, −z	10.21	−15.0	−3.9	−33.2	27.6	−30.6
	0	−x, −y, −z	7.92	−2.8	−0.2	−4.5	0.3	−6.9
	0	−x, −y, −z	18.87	2.9	−0.6	−4.7	1.5	−0.5

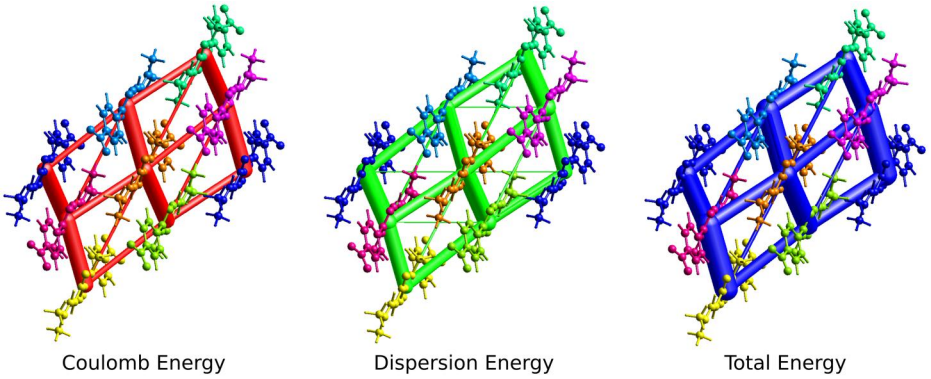

Figure 8. The energy frameworks of the compound along *c*-axis for Coulomb energy, dispersion energy and total energy terms.

selected molecule has been showing highest total interaction energy of −61.0 kJ/mol. The total interaction energy (−289 kJ/mol) comprising of electrostatic (−130.9 kJ/mol), polarization (−43.3 kJ/mol), dispersion (−277.2 kJ/mol), and repulsion (−198.4 kJ/mol) as per the energy evaluated by the interaction energy and 3D energy frameworks calculation. The molecule's energy frameworks for electrostatic, dispersion, and total energy terms were constructed and they were presented as different colored cylinders with a scale factor (cylinder tube size) of 150 and a cutoff energy of 50 kJ/mol. These cylinders show the strength of the molecular packing in various orientations as well as the size of the interaction energy between molecule pairs. The molecular cluster has blue cylinders for total interaction energy, green cylinders for dispersive energy, and red cylinders for electrostatic energy (Figure 8). The energy framework calculations demonstrated that in the crystal environment, the dispersion energy dominates the electrostatic and polarization energies.

3.5. DFT calculations

In accordance with the atom labeling in Figure 3, the optimized structural parameters determined using the basis set ωB97X/6-311++G(d,p) are provided in Table 6. As a result of potential energy scan, there are no imaginary frequencies were obtained for the optimized geometry. Therefore, molecule's optimized geometry is situated at the real minimum. The overlay of the experimental and theoretical structure yields rmsd value of 0.980 Å for the title compound as shown in Figure 9. The majority of the optimized bond lengths are somewhat longer than the experimental values, as shown in Table 6, and the bond angles are in excellent agreement with the experimental data. The torsion angles change slightly between the theoretical and experimental methods (Table 7). This is because theoretical calculations belong to isolated molecule in the gaseous phase while the experimental data belongs to molecule in crystalline phase.

3.5.1. Frontier molecular orbitals (FMO) analysis

As the basis for understanding the chemical stability and reactivity of organic components, the concepts of HOMO and LUMO are of fundamental prominence. The LUMO

Table 6. Comparison of selected bond lengths and bond angles obtained by XRD and DFT study.

	Bond length (Å)			Bond angle (°)	
Atoms	XRD	DFT	Atoms	XRD	DFT
O1–N1	1.216 (2)	1.230	O1–N1–O2	123.9 (2)	124.78
C1–C2	1.371 (2)	1.392	O1–N1–C1	118.14 (19)	117.61
N1–C1	1.470 (3)	1.470	N3–N2–C4	118.38 (12)	118.33
N2–N3	1.367 (2)	1.381	N3–N2–C7	111.06 (12)	110.57
N3–N4	1.2983 (19)	1.289	C4–N2–C7	130.54 (13)	131.07
N2–C7	1.3581 (17)	1.369	N2–N3–N4	107.06 (12)	107.17
C7–C8	1.384 (2)	1.388	N1–C1–C2	118.83 (18)	118.98
C11 –C12	1.355 (2)	1.364	C2–C1–C6	122.31 (17)	121.91
C7 –C9	1.484 (2)	1.493	O3–C10–C8	118.21 (14)	119.40
C10–C11	1.432 (2)	1.452	C12–N5–C14	121.09 (17)	120.81
O3–C10	1.2394 (18)	1.241	C10–C11–C12	119.05 (14)	118.44
N5–C14	1.451 (2)	1.454	C13–N5–C14	117.57 (17)	117.39

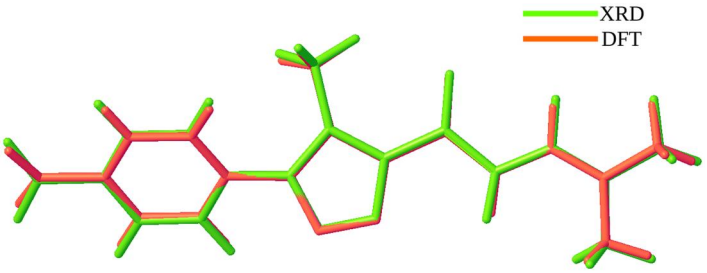

Figure 9. Superimposition of the structure of the triazole derivative obtained by XRD and DFT study.

Table 7. Comparison of selected torsion angles obtained by XRD and DFT.

	Angle (°)			Angle (°)	
Atoms	XRD	DFT	Atoms	XRD	DFT
O1–N1–C1–C2	165.1(2)	−179.54	C6–C1–C2–C3	0.4(3)	0.14
O1–N1–C1–C6	−15.3(2)	0.21	N1–C1–C6–C5	179.3(2)	179.42
O2–N1–-C1–C2	−15.1(3)	0.49	C2–C1–C6–C5	−1.1(3)	−0.82
O2–N1–C1–C6	164.6(2)	−179.75	C1–C2–C3–C4	0.9(2)	0.86
C4–N2–N3–N4	178.8(1)	178.76	C2–C3–C4–N2	179.9(2)	−179.81
C7–N2–N3–N4	0.3(2)	0.42	C2–C3–C4–C5	−1.6(2)	1.18
N3–N2–C4–C3	138.0(2)	143.86	N2–C4–C5–C6	179.5(1)	179.15
N3–N2–C4–C5	−40.6(2)	−34.80	C3–C4–C5–C6	1.0(2)	0.49

energy is immediately explained by the electron affinity, and the HOMO energy is directly explained by the ionization potential (IP). The energy gap, which refers to the energy difference between the HOMO and LUMO orbitals, is a crucial stability element for the molecule. The molecule with the smallest HOMO-LUMO gap is hence more reactive. Further, the higher the intermolecular interaction, the larger the dipole moment. The neutral atom with the highest potential for losing an electron is known as the ionization potential (IP). The frontier molecular orbitals (HOMO-LUMO), and their energy gap for all the compounds is shown in Figure 10, and their calculated chemical characteristics is reported in Table 8.

Thus, among all the compounds, molecule **C5** acts as a good electrophile as the molecule shows a slightly higher value for global electrophilicity index (ω) at 2.135 eV. To analyze the chemical behavior of these derivatives, we evaluated their global and reactive

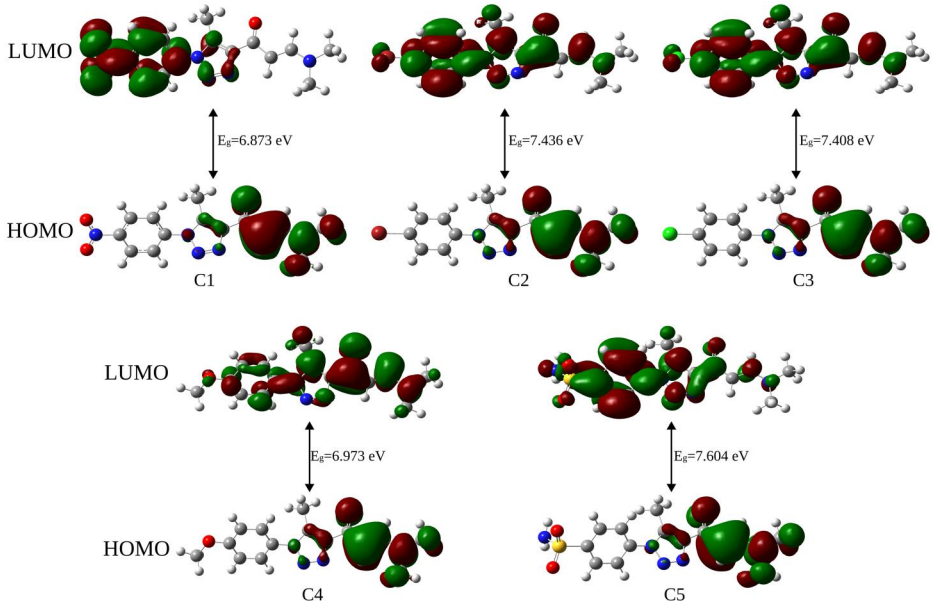

Figure 10. FMO diagram of all the compounds.

Table 8. The energy values of FMOs and their global reactive parameters of all the compounds.

Parameters	C1	C2	C3	C4	C5
E_{HOMO}	−7.653 eV	−7.711 eV	−7.710 eV	−7.589 eV	−7.831 eV
E_{LUMO}	−0.280 eV	0.276 eV	0.302 eV	0.616 eV	−0.228 eV
Energy gap (ΔE)	6.873 eV	7.436 eV	7.408 eV	6.973 eV	7.604 eV
Ionization energy (I)	7.653 eV	7.711 eV	7.710 eV	7.589 eV	7.831 eV
Electron affinity (A)	0.280 eV	−0.276 eV	−0.302 eV	−0.616 eV	0.228 eV
Electronegativity (χ)	3.618 eV	3.718 eV	3.704 eV	3.486 eV	4.030 eV
Chemical potential (μ)	−3.618 eV	−3.718 eV	−3.704 eV	−3.486 eV	−4.030 eV
Global hardness (η)	4.069 eV	3.993 eV	4.006 eV	4.102 eV	3.802 eV
Global softness (s)	0.258 eV^{-1}	0.250 eV^{-1}	0.250 eV^{-1}	0.244 eV^{-1}	0.263 eV^{-1}
Electrophilicity index (ω)	1.531 eV	1.731 eV	1.410 eV	1.481 eV	2.135 eV

parameters. The values of μ, χ, S, η and ω were calculated and the results are listed in supplementary Table 8. The global hardness value of the compound **C2** is lesser compared to all other molecules. Hence, molecule **C2** is more reactive than all the compounds. Further, the molecule **C5** has a higher electronegativity value ($\chi = 4.030$), hence, it is the best electron acceptor.

3.5.2. Molecular electrostatic potential (MEP) analysis

A three-dimensional diagram called MEP map can be used to see how the molecules' reactive sites and charges are distributed. It is helpful in biological recognition processes and hydrogen bonding interactions and serves as an example of feasible places for electrophilic and nucleophillic attacks. With the aid of this computation, the polarity of the molecule can also be understood visually. The color scale depicts the region of the molecule's surface with the highest electrostatic potential; red signifies this region, blue the region with the highest positive electrostatic potential, and green the region with the lowest potential. The electrostatic potential value ascends in the order red < green < blue [25].

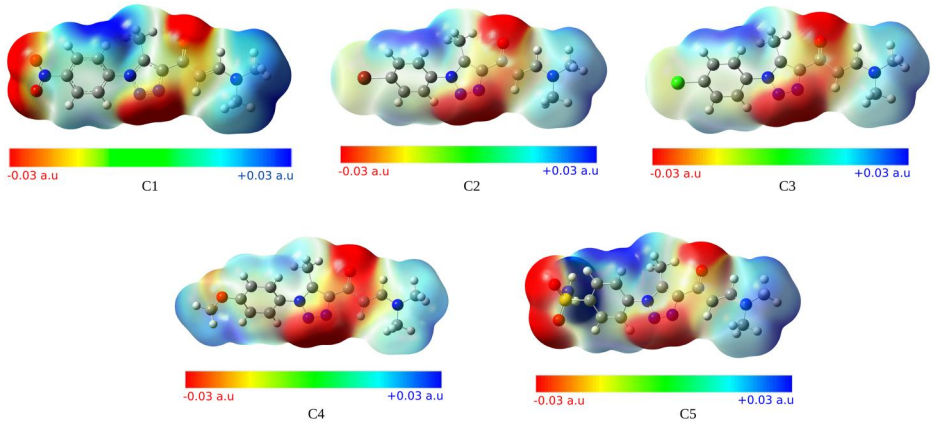

Figure 11. MEP map of all the compounds.

Figure 11 displays the MEP map of the five chosen triazole derivatives. From the diagram, it can be seen that the positive electrostatic potential corresponds to the repulsion of a proton by the nucleus (red region) and the negative electrostatic potential corresponds to the attraction of a proton by the cluster of electron density in the molecule (blue region). The color scale of the presented MEP ranges from −0.03 to +0.03 a.u. Figure 11 clearly reveals that the negative regions are concentrated around the oxygen atoms of the nitro group, carbonyl group, and around the nitrogen atoms of the triazole ring whereas most positive regions are around the hydrogen atoms which are most reactive sites for a nucleophillic attack. These regions are responsible for the existence of inter-molecular interactions in the compound and behave as donor and acceptor regions.

3.5.3. QTAIM and NCI analyses

To comprehend the inter- and intra- molecular interactions inherent in the molecules, the quantum theory of atoms in molecules (QTAIM) is carried out. The regions of the non-covalent interactions are graphically visualized owing to the NCI-RDG analysis. The RDG isosurfaces and 2D scatter plots with the surface color of blue-green-red have the advantage of making it easier to see how they relate to one another. Sign $(\lambda_2)\rho$ is a measure of the attractiveness or repulsiveness of an interaction. Sign $(\lambda_2)\rho > 0$ indicates a repulsive interaction, Sign $(\lambda_2)\rho < 0$ indicates an attractive interaction, and Sign $(\lambda_2)\rho$ equal to zero indicates a weak van der Waals interaction [26]. The QTAIM analysis for five triazole derivatives was established to search all (3, -1) bond critical paths (BCP). The paths generated are shown in Figure 12a. The presence of BCP corresponding to C-H … C and C–H … O validates intramolecular interactions present in the experimental structure. The QTAIM analysis does not include some weak non-covalent interactions since it only considers bond critical points in the electron density. To overcome this problem the NCI index is used since it is based on the reduced density gradient (RDG), which is a function of the electron density $\rho(r)$ and its first derivative $\nabla\rho(r)$.

In Figure 12 the red spikes indicate the steric repulsion noticed in the centers of benzene and triazole ring which is due to the steric repulsive force between the carbon atoms present in the rings. The mixed red-green colored spikes observed near the

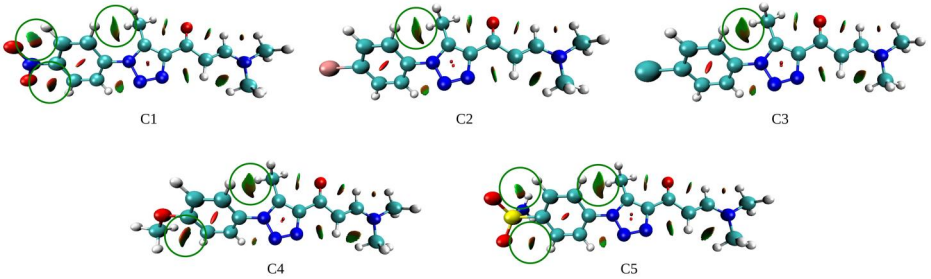

Figure 12. 3D RDG-NCI isosurfaces of all the molecules.

aromatic rings and the attached substituents indicate the attractive interaction between the hydrogen atoms and the other atoms. The absence of blue colored isosurface in the 3D NCI isosurface and blue peaks in the 2D scattered map indicates that there is no strong hydrogen bond interaction in the molecule.

4. Conclusions

The present report aims to shed a light on structure investigation of a triazole derivative. The synthesized molecule is subjected to FTIR, NMR and XRD analyses. Structural analysis revealed that nitrobenzene group is slightly deviates from the mean plane. The C–H … O and C–H … N intermolecular interactions are mainly responsible for the crystal packing of the title molecule. Hirshfeld surface analysis visualized the presence of intermolecular interactions in the molecule. The various interaction energies like electrostatic, dispersion, polarization, repulsion energies are calculated using 3D energy framework calculations and it was found that dispersion energy dominates the other two energies. DFT calculations validate the geometry of the structure of the molecule. FMO analysis revealed that the HOMO-LUMO energy gap was found to be 2.869 eV. MEP analysis unveiled the reactive sites present in the molecule. Further, QTAIM and NCI analyses corroborate the weak interactions present in the molecule. FMO, MEP, QTAIM and NCI studies of four related compounds shows that triazole derivatives have reactive sites which make them potential candidates for pharmaceutical applications.

Acknowledgments

Authors are grateful to Prof. N. K. Lokanath, Department of Studies in Physics, University of Mysore, Mysuru and Dr. S. Naveen, Scientific Officer, IoE, Vijnana Bhavan, University of Mysore, Mysuru for their help in collection of single crystal X-ray diffraction data. The single crystal X-ray diffraction facility used for data collection was funded by the Ministry of Human Resource Development (MHRD), Government of India, under Institute of Excellence (IoE) Scheme sanctioned to the University of Mysore, Mysuru, India.

Disclosure statement

The authors declare that they have no known competing financial interests or personal relationships that could have appeared to influence the work reported in this paper.

Funding

This work is supported by the University Grants Commission (UGC), India, under Major Research Project Scheme [F.No.41–882/2012 (SR)].

ORCID

M. K. Usha http://orcid.org/0000-0001-6605-3605
T. N. Lohith http://orcid.org/0000-0003-1808-740X
M. A. Sridhar http://orcid.org/0000-0002-3065-3630

References

[1] S. M. Riyadh *et al.*, *Heterocycles* **75** (8), 1849 (2008). DOI: 10.3987/REV-07-625.
[2] A.-Z. A. Elassar, and A. A. El-Khair, *Tetrahedron* **59** (43), 8463 (2003). DOI: 10.1016/S0040-4020(03)01201-8.
[3] K. V. Sujith *et al.*, *Med. Chem. Res.* **21** (5), 543 (2012). DOI: 10.1007/s00044-011-9569-5.
[4] A. M. Isloor, B. Kalluraya, and P. Shetty, *Eur J. Med Chem.* **44** (9), 3784 (2009). DOI: 10.1016/j.ejmech.2009.04.038.
[5] N. Boechat *et al.*, *J. Chem. Crystallogr.* **46** (6-7), 296 (2016). DOI: 10.1007/s10870-016-0659-6.
[6] S. Manfredini *et al.*, *Bioorg. Med. Chem.* **8** (9), 2343 (2000). DOI: 10.1016/s0968-0896(00)00160-7.
[7] G. Biagi *et al.*, *Farmaco* **59** (5), 397 (2004). DOI: 10.1016/j.farmac.2004.01.012.
[8] S. Shetty *et al.*, *Indian J. Heterocycl. Chem.* **23** (3), 33 (2013).
[9] A. Bruker, *APEX2* (Bruker A.X.S. Inc., Madison, Wisconsin, USA, 2012).
[10] G. M. Sheldrick, *Acta Crystallogr. C Struct. Chem.* **71** (Pt 1), 3 (2015). DOI: 10.1107/S2053229614024218.
[11] A. L. Spek, *J. Appl. Crystallogr.* **36** (1), 7 (2003). DOI: 10.1107/S0021889802022112.
[12] C. F. Macrae *et al.*, *J. Appl. Crystallogr.* **53** (Pt 1), 226 (2020). DOI: 10.1107/S1600576719014092.
[13] P. R. Spackman *et al.*, *J. Appl. Crystallogr.* **54** (Pt 3), 1006 (2021). DOI: 10.1107/S1600576721002910.
[14] S. L. Tan, M. M. Jotani, and E. R. T. Tiekink, *Acta Crystallogr. E Crystallogr. Commun.* **75** (Pt 3), 308 (2019). DOI: 10.1107/S2056989019001129.
[15] M. A. Spackman, and D. Jayatilaka, *Cryst. Eng. Comm.* **11** (1), 19 (2009). DOI: 10.1039/B818330A.
[16] C. F. Mackenzie *et al.*, *IUCrJ* **4** (Pt 5), 575 (2017). DOI: 10.1107/S205225251700848X.
[17] N. L. Rani *et al.*, *Mol. Cryst. Liq. Cryst.* **607** (1), 223 (2015). DOI: 10.1080/15421406.2014.928978.
[18] T. N. Lohith *et al.*, *J. Mol. Str* **1252**, 132203 (2022). DOI: 10.1016/j.molstruc.2021.132203.
[19] M. J. Frisch *et al.*, *Gaussian 09, Revision A.01* (Gaussian, Inc., Wallingford, 2009).
[20] R. Dennington, T. A. Keith, and J. M. Millam, *GaussView, Version 6.0*, John M. (Semichem Inc., Shawnee Mission, KS, 2016).
[21] C. Burudeghatta Sundaramurthy *et al.*, *Mol. Syst. Des. Eng.* **7** (2), 132 (2022). DOI: 10.1039/D1ME00113B.
[22] T. Lu, and F. Chen, *J. Comput. Chem.* **33** (5), 580 (2012). DOI: 10.1002/jcc.22885.
[23] W. Humphrey, A. Dalke, and K. Schulten, *J. Mol. Graph* **14** (1), 33 (1996). DOI: 10.1016/0263-7855(96)00018-5
[24] K. M. Chandini *et al.*, *J. Mol. Str.* **1244**, 130910 (2021). DOI: 10.1016/j.molstruc.2021.130910.
[25] T. N. Lohith *et al.*, *J. Mol. Str.* **1267**, 133476 (2022). 133476. DOI: 10.1016/j.molstruc.2022.133476.
[26] N. Latha Rani *et al.*, *Mol. Cryst. Liq. Cryst.* **624** (1), 262 (2016). DOI: 10.1080/15421406.2015.1038032.